Supplementary Information for

Synergistic dispersal of plant pathogen spores by jumping-droplet condensation and wind

Ranit Mukherjee[1], Hope A. Gruszewski[2], Landon T. Bilyeu[2], David G. Schmale III[2], and Jonathan B. Boreyko[3,*]

[1]Department of Biomedical Engineering and Mechanics, Virginia Tech, Blacksburg, VA 24061, USA.
[2]School of Plant and Environmental Sciences, Virginia Tech, Blacksburg, VA 24061, USA.
[3]Department of Mechanical Engineering, Virginia Tech, Blacksburg, VA 24061, USA.

This PDF file includes:

Figures S1–S13
Supplementary Text (Sections 2–5)
Captions for Video S1 and S2

*e-mail: boreyko@vt.edu

1 Supporting figures

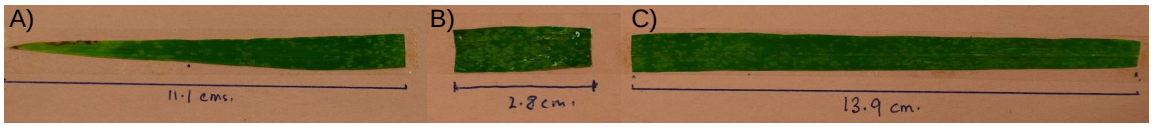

Figure S1: Dimensions of a healthy wheat leaf cut from the stem. (A) The tip section is of variable width. (B) In the middle section, the leaf width is almost uniform ($\approx$1 cm). This $\approx$3 cm long middle section was used for all of the experiments. (C) The leaf again tapers off toward the end near the stem.

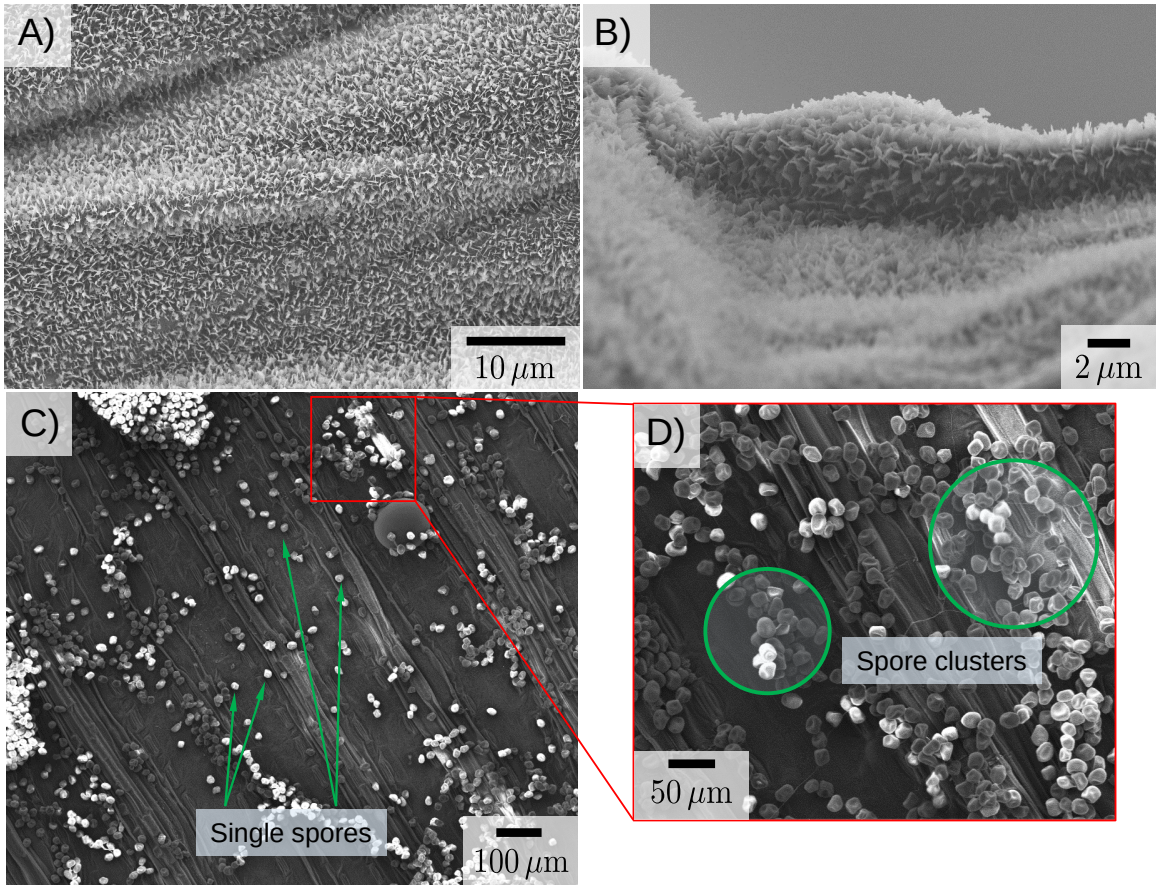

Figure S2: Scanning electron micrograph (SEM) images of a healthy wheat leaf with (A) 5 kX magnification and (B) 10 kX magnification. The nanometric surface asperities on the top surface of the leaves, clearly visible in these images, are generally coated with wax which render the wheat leaves superhydrophobic. (C) SEM images of single spores and spore clusters on a diseased wheat leaf (top surface). (D) Careful examination of the spores in the magnified image confirms that they are adhered to the leaf surface.

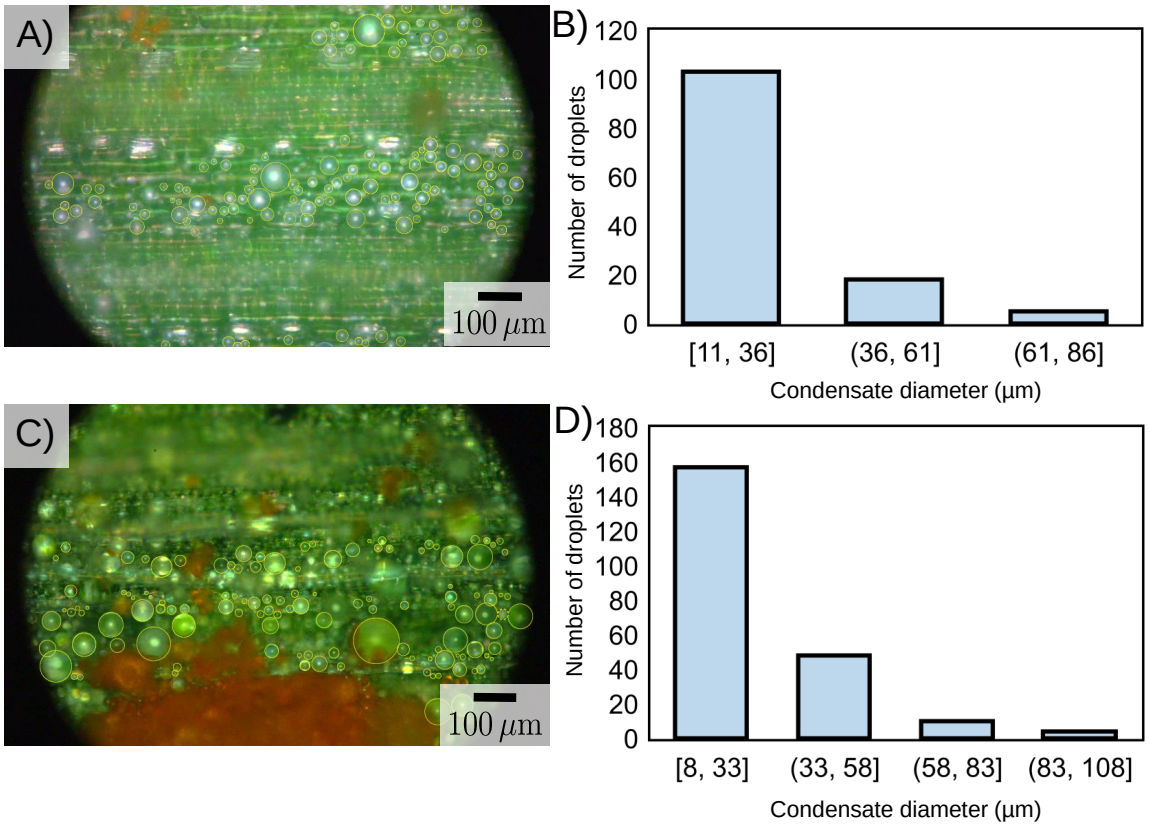

Figure S3: (A, C) Optical microscope images of typical steady-state condensate growth pattern on the top surface of a diseased wheat leaf. The condensates which are in focus are demarcated with yellow borders. (B, D) Distribution of the dew droplet diameters from the leaf in image (A) and (C), respectively. While majority of the droplets are within 40 μm, a considerable number of droplets are in the 60-110 μm range.

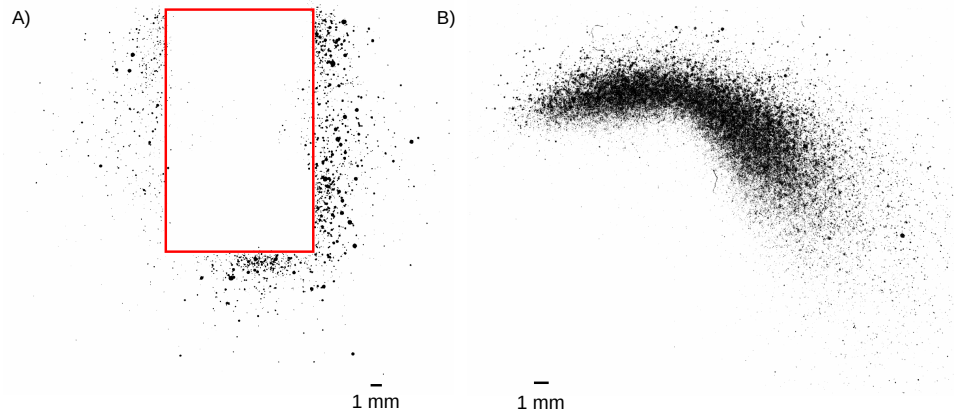

Figure S4: (A) Typical stain pattern on a water-sensitive paper after 1 h of continuous condensation on an overlying leaf for the no-wind condition. ImageJ thresholding and segmentation analysis were used to separate the droplet patterns (black dots) from the background. In this particular case, the number of condensates which impacted the paper was 1,914. The average number of condensates captured on a paper for the no-wind experiments is $2,800 \pm 1,800$. This number is much less than the actual number of droplets jumping off the leaf after coalescence, as only a subset of jumping droplets cleared the edge of the wheat leaf for the no-wind condition. The red border shows the stage where the leaf section was attached over the water-sensitive paper. Some black dots (condensate pattern) can also be seen directly under the leaf which can be explained by the very small size of these droplets and existence of a small wind non-detectable by our anemometer, as stated elsewhere in the text. (B) To get a better estimate of the amount of jumped droplets in an hour-long experiment, results from the perpendicular paper tests with wind were used. Due to the large number of droplets overlapping on the paper, the measurement was difficult. Nonetheless, for a 1 h trial with 1.5 m/s wind speed, about 29,800 condensates were measured on the paper. Some negative errors in this measurement were likely due to the overlapping patterns.

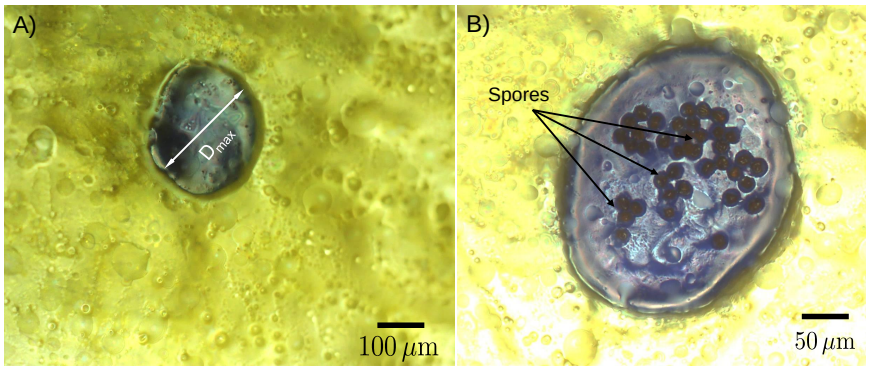

Figure S5: (A) Magnified view of a blue stain caused by a jumping dew droplet landing on water-sensitive paper (yellow). No spores were inside of this particular jumped droplet. The maximum diameter of the stain ($D_{\max}$), shown here, was used for Eq. 1 in the main manuscript. (B) Another example of a stain from a jumped droplet, where in this case there were 39 spores adhered to the droplet. In both cases, there was no wind above the diseased leaf, such that the droplets jumped over the edge of the leaf onto the underlying paper.

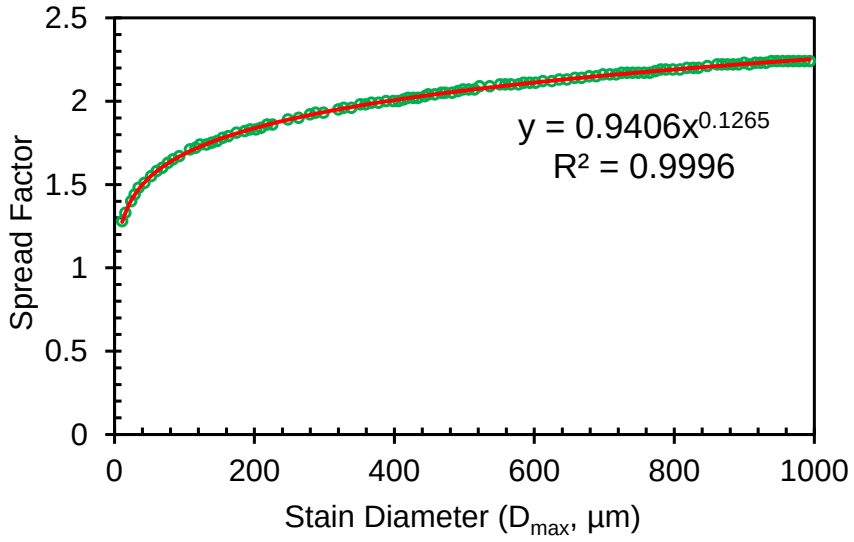

Figure S6: Spread factor of water droplets on the water-sensitive papers, defined as the ratio of the maximum stain diameter ($D_{\max}$) to the pre-impact droplet diameter. The green data points are extracted from the product datasheet by using a plotting software (WebPlotDigitizer). The smooth red curve is the fitted power-law which was used to obtain the spread factor corresponding to any given stain diameter.

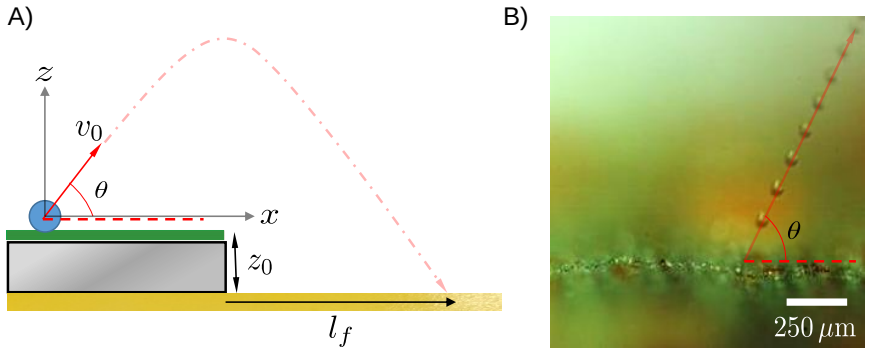

Figure S7: (A) Schematic of the projectile motion of a droplet jumping off the leaf. The coordinate axes ($x - z$), jumping velocity (v_0), the angle of the jump (θ), and the trajectory of the airborne droplet is shown. The vertical distance between the leaf and the water-sensitive paper is shown by z_0 which is 1 cm. The distance of the stains on the paper from the edge of the leaf is shown by l_f which is the same as that shown in Fig. 2a in the main text. (B) Chronophotograph of a jumping droplet from a diseased wheat leaf is shown along with the jumping angle θ. Successive positions of the jumped droplet are temporally separated by 40 μs.

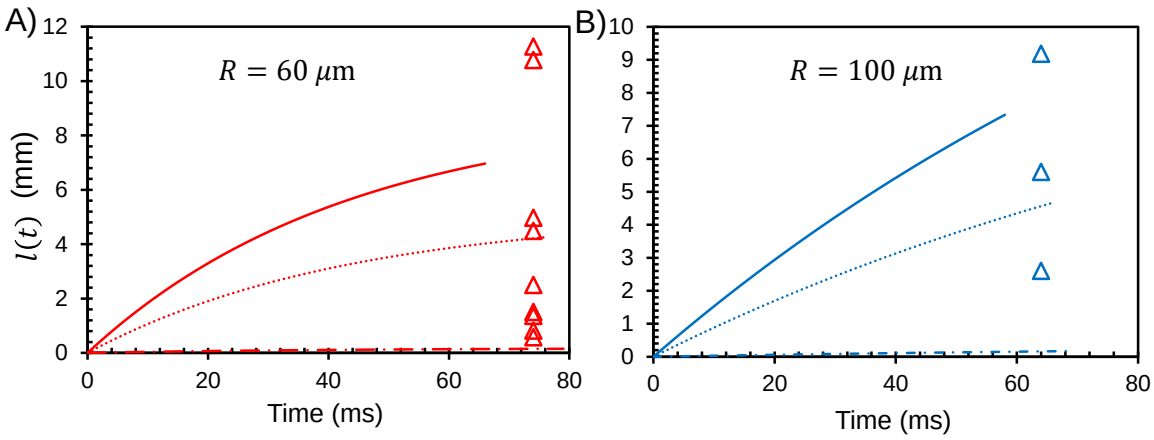

Figure S8: (A,B) The lateral displacement versus time for a jumping droplet of radius $R = 60\,\mu$m, and $100\,\mu$m, respectively. Each graph shows the displacement curves for three different jumping angles with respect to the horizontal: 30° (solid curve), 60° (dotted), and 89° (dash-dotted). The maximum lateral displacement for a jumped droplet (l_f) is represented by the terminal end of each curve. The value of l_f corresponds to the critical time when the projectile motion equation predicts the droplet will impact on the water-sensitive paper below (mimicking a neighboring leaf). For these plots, the paper was placed 1 cm beneath the leaf. Experimental values of l_f are also overlaid on the same plot as symbols. The jumped droplet radius were calculated from the stain diameters on the papers via the spread factors (see Section 2). Although the majority of the experimental data points fall within the theoretical limits, some droplets did travel farther than the theoretical l_f. This can be explained by droplets getting boosted by the air circulation in the laboratory, as can be seen in Supporting Video S1 where the lateral displacement of jumping droplets is several times larger during the downward descent compared to the upward launch. This air circulation was quite mild, as it was less than the 0.4 m/s resolution of the anemometer, but this is sufficient in the context of affecting micrometric droplets.

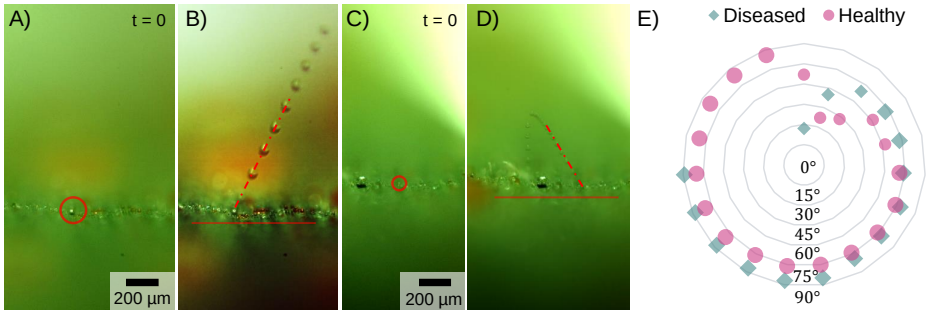

Figure S9: (A) Condensates forming near one of the microbumps on the top surface of a diseased leaf. (B) Chronophotograph of the jumped droplet trajectory shows that the jumping angle was less than 90°. (C) While the microbumps are not apparent in this image, the successive jumping in figure (D) shows the directional jumping at an angle much less than 90°. (E) We tracked the trajectory of several droplets jumping off diseased and healthy wheat leaves and plotted the jumping angles (angle θ in Fig. S7) on a radar chart. Boundaries of the concentric circles on the radar chart represent angles at an interval of 15° with the center being 0°. In more than 76% cases (bigger data points), the jumping angle was between 70°-90°, *i.e.* within the last two concentric circles.

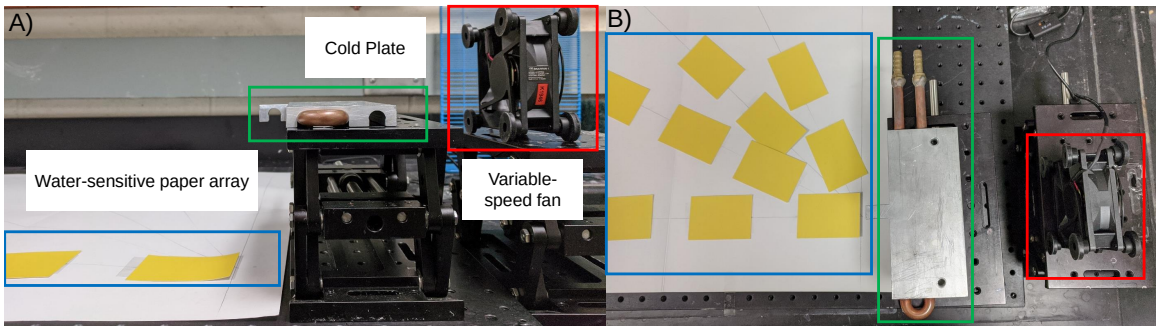

Figure S10: Experimental setup to understand the synergystic effect of wind and condensation. (A) Side-view of the setup with the variable-speed axial fan, cold plate with the overhang, and the water-sensitive paper array ($\alpha = 0°$). (B) Top-view of the setup with paper arrays placed in different angles.

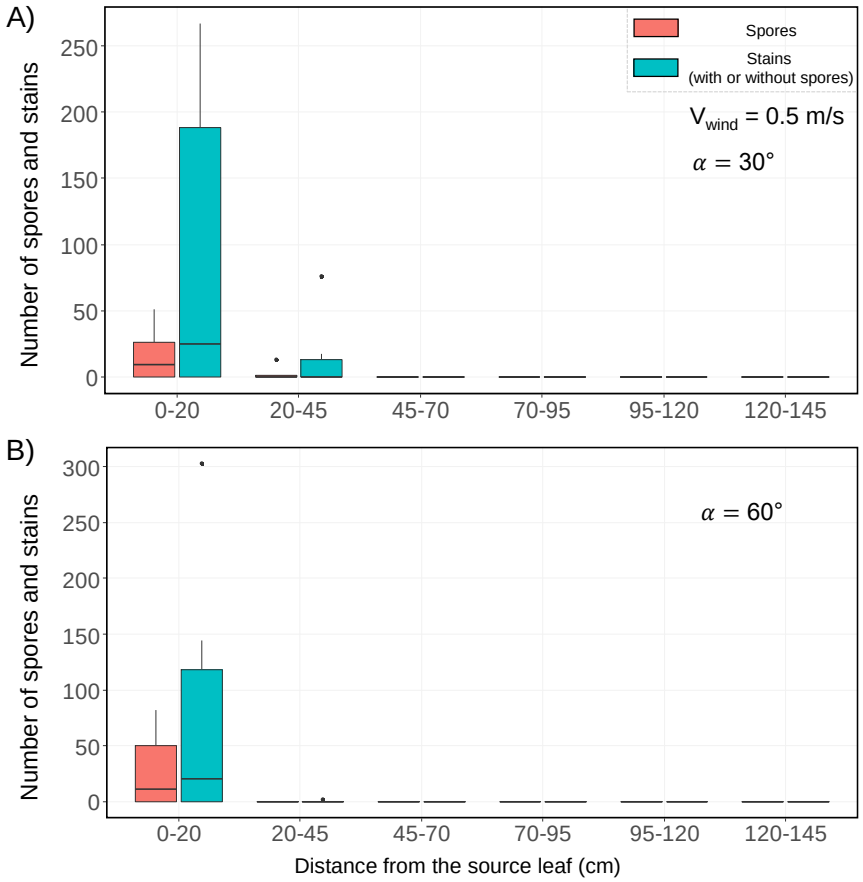

Figure S11: The number of impacted droplets (with or without spores) and the number of spores per paper are plotted against the distance from the source leaf for $V_{\text{wind}} = 0.5\,\text{m/s}$. All distances are measured along the (A) $\alpha = 30°$ and (B) $\alpha = 60°$ lines. No droplets were captured on the papers placed along the $\alpha = 45°$ line.

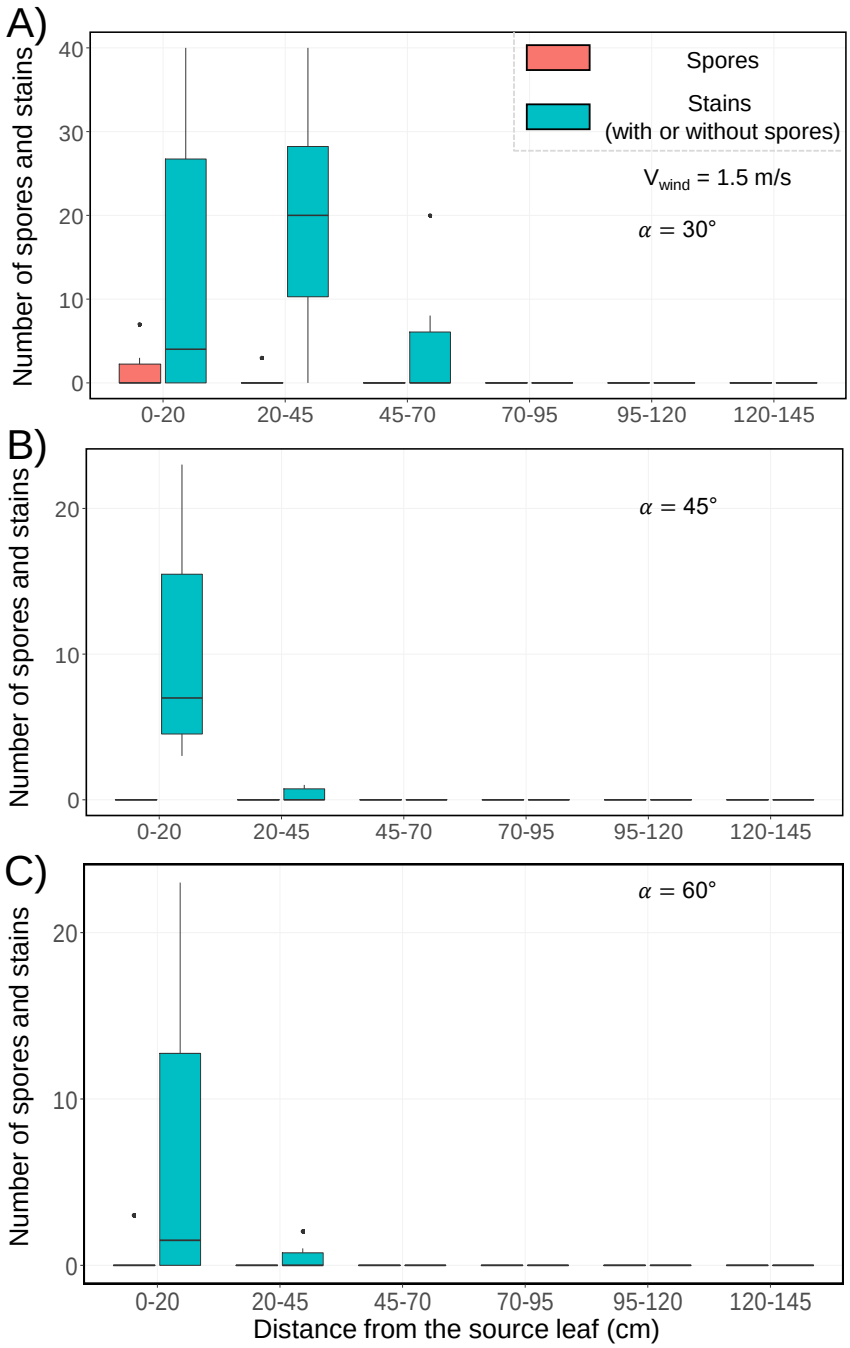

Figure S12: The number of impacted droplets (with or without spores) and number of spores per paper are plotted against the distance from the source leaf for $V_{\text{wind}} = 1.5\,\text{m/s}$. All distances are measured along the (A) $\alpha = 30°$, (B) $\alpha = 45°$, and (C) $\alpha = 60°$ lines.

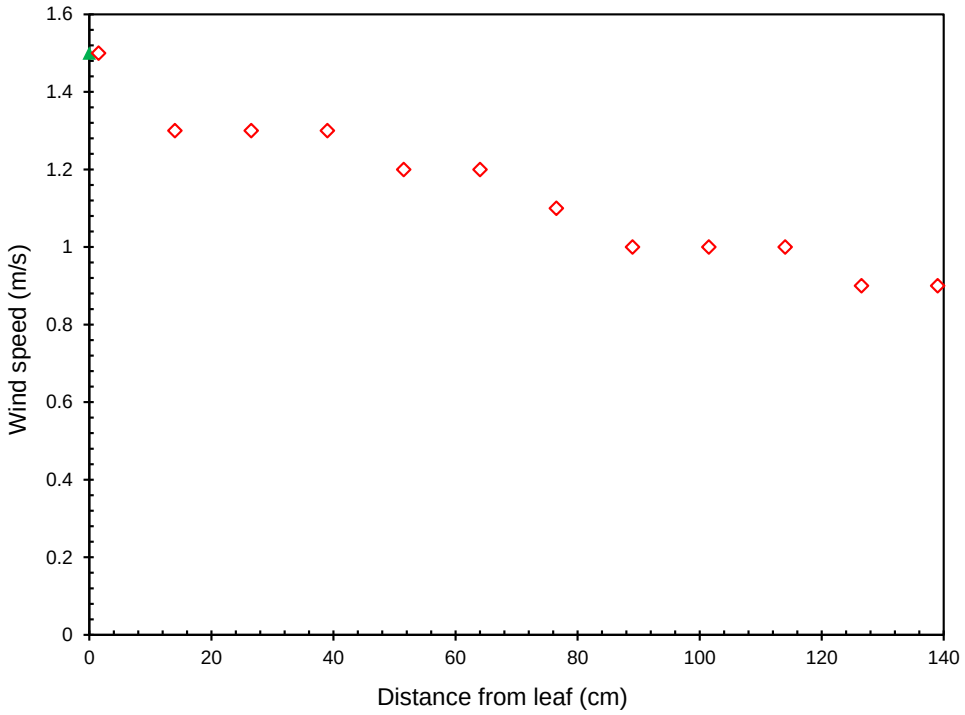

Figure S13: Spatial variation of the wind speed, as measured 1 cm above the array of water-sensitive papers. This plot is only for the papers placed along the $\alpha = 0°$ line downstream of the leaf. The green triangle indicates the wind speed ($V_{\text{wind}} = 1.5\,\text{m/s}$) 1 cm above the leaf. A similar plot is not available for $V_{\text{wind}} = 0.5\,\text{m/s}$, as equivalent drop in the wind velocity with distance resulted in a wind speed lower than 0.3 m/s, below the minimum measurable value for the anemometer used in our study.

2 General discussion on leaf morphology and jumping-droplet condensation

Wheat leaves are superhydrophobic in nature, as shown by the quasi-spherical condensing droplets in the inset of Fig. 4C in the main text. More detailed contact angle measurements in previous reports also point towards such superhydrophobicity [1, 2]. The superhydrophobic jumping-droplet effect is enabled by the nanometric surface asperities on the leaf surface (Fig. S2), which are coated with leaf wax. Coalescence-induced droplet jumping has been observed on both artificial [3–6] and natural substrates [7–9] comprised of nanostructures or hierarchical micro/nano-structures [10]. During the initial stages of condensation, nanometric ($\approx 1-10\,\text{nm}$ for water) embryos tend to nucleate within the nano-roughness [4, 6]. How these nanometric embryos grow within the cells surrounded by the nanotextures dictates the condensation-induced adhesion as well as occurrence of droplet jumping. If the embryos grow laterally and fill the texture voids before protruding upwards, highly adhesive Wenzel droplets are formed. On the other hand, the jumping-droplet effect is observed when these nucleating embryos can stably inflate into a Cassie state without flooding the surface textures beneath [5, 6]. Naturally, only the Cassie (or partial Cassie) wetting morphologies show jumping-droplet condensation. Thus, the degree of droplet adhesion to the surface (i.e. Wenzel state *vs.* Cassie state) is the more important indicator of the ability to promote jumping-droplet condensation, as opposed to a simple measurement of a droplet's contact angle [5].

The above general discussion sheds some light into how the wax-coated hierarchical nanostructured geometry in both wheat and lotus leaves [9] gives rise to the superhydrophobicity and jumping-droplet condensation behavior. As a natural extension to this, other plant surfaces with hierarchical features should also exhibit similar condensate jumping behavior. Indeed, Mockenhaupt et al. observed coalescence-induced dislodging of dew droplets on the superhydrophobic leaves of eight different plants [9, 11]. Extensive lists of plant surfaces with varying degrees of hierarchical micro and nano-textures has been compiled by Barthlott et al. [12,13] which can be useful for future studies looking into the importance of dew formation in fungal pathogen transport in other plants.

3 Determining the spread factor for the stains on the water-sensitive papers

The pre-impact droplet diameter D of a jumped droplet (with or without spores) can be computed from the maximum stain diameter ($D_{\max}$) on the water-sensitive paper. Figure S5 shows the relation between the spread factor $D_{\max}$ for water droplets at 20 °C ambient condition and 40% relative humidity, where the spread factor is $D_{\max}/D$. The relative humidity of the ambient has no discernible effect on the relation. These measurements were extracted from the water-sensitive paper datasheet which states that the spread factor values were assessed by the magnesium oxide method. Once the experimental plot points were extracted, a smooth power law curve was fitted over the data points to find the function which was used to find the spread factor for any given $D_{\max}$.

4 Derivation of the projectile motion of a jumped droplet (without air flow)

The equation of motion for a droplet jumping off the leaf at an angle θ and initial jumping velocity $u = 0.22(\gamma/\rho R)^{1/2}$ is given by:

$$m\frac{du_x(t)}{dt} = -cu_x(t), \tag{S1}$$

$$m\frac{du_z(t)}{dt} = -mg - cu_z(t), \tag{S2}$$

where $m = (4/3)\rho_w \pi R^3 g$ is the mass of the water droplet of density ρ_w and radius R, $c = 6\pi\mu R$ is the Stokes drag coefficient, and $v_x(t)$ and $v_z(t)$ are the x and z components of velocity of the airborne droplet. The assumption of Stokes drag is borne out when considering the Reynolds number ($Re = 2\rho_{air} uR/\mu_{air}$) for the flow around the droplet is low for the range of R values chosen here ($Re \approx 1.6 - 3.2$). By defining $k := c/m$, we can rewrite the above differential equations as-

$$\frac{d}{dt}\begin{pmatrix} u_x \\ u_z \end{pmatrix} = \frac{d}{dt}\begin{pmatrix} -ku_x \\ -g - ku_z \end{pmatrix} \tag{S3}$$

Using the initial conditions $u_x(0) = u\cos\theta$, $u_z(0) = u\sin\theta$, we can solve for the horizontal and the vertical position of the jumped droplet as a function of time-

$$x(t) = \frac{u_x(0)}{k}(1 - e^{-kt}) \tag{S4}$$

$$z(t) = -\frac{g}{k}t + \frac{1}{k}\left(u_z(0) + \frac{g}{k}\right)(1 - e^{-kt}) \tag{S5}$$

By choosing a value for the droplet radius R, we can plot $x(t) \equiv l(t)$ lines for different values of the jumping angle $\theta = 30°, 60°, 89°$, as shown in Fig. 2c in main text and in Fig. S4. We can also solve for the total time of flight (t_c) for a droplet of radius R by using $z = -0.01$ m in Eq. S5, which accounts for the droplet returning to the water sensitive paper $y_0 = 1$ cm below the leaf. Three different t_c values were obtained corresponding to the three different θ where the corresponding curves were end.

5 Critical speed of removal of dry spores from wheat leaves

The hydrodynamic force exerted by wind with a mean speed of U, on a spherical spore of radius R_p, can be defined as-

$$F_{shear} \approx 1.7 \times 6\pi\mu_a \dot{\gamma} {R_p}^2, \tag{S6}$$

where μ_a is the viscosity of air and $\dot{\gamma} \approx U/\delta$ is the velocity gradient within a boundary layer of thickness δ [14]. The boundary layer thickness is again related to the leaf section size x and the free stream wind speed U as $\delta \sim \left(\frac{\nu x}{U}\right)^{1/2}$. This shear force has to overcome the adhesion force exerted by the surface on the particle. For a completely dry leaf with uncharged spores, this adhesion force is mainly due to the van der Waals force:

$$F_{vdW} \approx (A/6z^2)R_p, \tag{S7}$$

where A is the Hamaker constant and z is the closest possible separation distance between the awn surface and the spore [15]. For most organic molecules, $A \sim 10^{-20}$ J [15] and z is taken as 1 nm due to the nanoscopic surface asperities.

The theoretical critical wind speed for the removal of the dry spores ($R_p \sim 10\,\mu$m) can then be found by combining all of the above equations:

$$U_c = \left(\frac{(A/6z^2)}{1.7 \times 6\pi\mu_a R_p (\nu x)^{-1/2}}\right)^{2/3}, \tag{S8}$$

which comes out to be about 10 m/s taking $x \sim 1$ cm which is in general the width of a wheat leaf, and $\mu_a = 1.81 \times 10^{-5}$ Pa·s and $\nu = 1.5 \times 10^{-5}$ m^{2}s^{-1}. While this is larger than the experimental threshold

wind speed for dry spore removal [16], this discrepancy comes from the assumption of a fixed Hamaker constant and the separation distance values. A Hamaker constant of $A \sim 10^{-21}$ J, which is still within the acceptable range of values for a wide varitey of surface and particle combination and a slightly increased separation distance of 2 nm gives $U_c \approx 2.9$ m/s which is very close to the experimental critical wind speed value reported in Ref. [16].

6 Video captions

Video S1: Coalescence-induced droplet jumping on a healthy wheat leaf. The jumped droplet easily cleared the boundary layer and deposited beyond the leaf edge, even in the absence of any detectable wind.

Video S2: Coalescence of condensing droplets on a fungicide-sprayed healthy wheat leaf. The hydrophilic contact angles of the condensed droplets are visible in the video which resulted in the suppression of coalescence-induced jumping phenomenon. In both videos, typically the surface of the wheat leaf was held at 1 °C, while the air temperature was $T_\infty = 21$°C and humidity was $H = 43\%$.

References

[1] S. Nath, S. F. Ahmadi, H. A. Gruszewski, S. Budhiraja, C. E. Bisbano, S. Jung, D. G. Schmale III, and J. B. Boreyko. 'sneezing' plants: pathogen transport via jumping-droplet condensation. *J. Royal Soc. Interface*, 16, 2019.

[2] H. Park, S. Kim, H. A. Gruszewski, D. G. Schmale III, J. B. Boreyko, and S. Jung. Dynamics of splashed droplets impacting wheat leaves treated with a fungicide. *J. Royal Soc. Interface*, 17:20200337, 2020.

[3] J. B. Boreyko and C. H. Chen. Self-propelled dropwise condensate on superhydrophobic surfaces. *Phys. Rev. Lett.*, 103:184501, 2009.

[4] M. D. Mulroe, B. R. Srijanto, S. F. Ahmadi, C. P. Collier, and J. B. Boreyko. Tuning superhydrophobic nanostructures to enhance jumping-droplet condensation. *ACS Nano*, 1:8499—8510, 2017.

[5] T. Mouterde, Gaélle Lehoucq, Stéphane Xavier, A. Checco, C. T. Black, A. Rahman, T. Midavaine, C. Clanet, and D. Quéré. Antifogging abilities of model nanotextures. *Nat. Mater.*, 16:658–663, 2017.

[6] N. Miljkovic, R. Enright, and E. N. Wang. Effect of droplet morphology on growth dynamics and heat transfer during condensation on superhydrophobic nanostructured surfaces. *ACS Nano*, 6:1776–1785, 2012.

[7] J. B. Boreyko and C. H. Chen. Restoring superhydrophobicity of lotus leaves with vibration-induced dewetting. *Phys. Rev. Lett.*, 103:174502, 2009.

[8] K. M. Wisdom, J. A. Watson, X. Qu, F. Liu, G. S. Watson, and C. H. Chen. Self-cleaning of superhydrophobic surfaces by self-propelled jumping condensate. *Proc. Natl. Acad. Sci. U.S.A.*, 110:7992–7997, 2013.

[9] G. S. Watson, M. Gellender, and J. A. Watson. Self-propulsion of dew drops on lotus leaves: a potential mechanism for self cleaning. *Biofouling*, 30:427–434, 2014.

[10] X. Chen, R. S. Patel, J. A. Weibel, and S. V. Garimella. Coalescence-induced jumping of multiple condensate droplets on hierarchical superhydrophobic surfaces. *Sci. Rep.*, 6:18649, 2016.

[11] B. Mockenhaupt, H. J. Ensikat, M. Spaeth, and W. Barthlott. Superhydrophobicity of biological and technical surfaces under moisture condensation: stability in relation to surface structure. *Langmuir*, 24:13591–13597, 2008.

[12] C. Neinhuis and W. Barthlott. Characterization and distribution of water-repellent, self-cleaning plant surfaces. *Annals of Botany*, 79:667–677, 1997.

[13] K. Koch and W. Barthlott. Superhydrophobic and superhydrophilic plant surfaces: an inspiration for biomimetic materials. *Phil. Trans. R. Soc. A*, 367:1487–1509, 2009.

[14] M. Sokuler, G. K. Auernhammer, C. J. Liu, E. Bonaccurso, and H. J. Butt. Dynamics of condensation and evaporation: Effect of inter-drop spacing. *Europhys. Lett.*, 89(3):36004, 2010.

[15] J. N. Israelachvili. *Intermolecular and surface forces.* Academic Press, 1990.

[16] L. Geagea, L. Huber, and I. Sache. Removal of urediniospores of brown (puccinia recondita f.sp. tritici) and yellow (p. striiformis) rusts of wheat from infected leaves submitted to a mechanical stress. *Eur. J. Plant Pathol.*, 103:785–793, 1997.